Mechanistic DNA damage simulations in Geant4-DNA part 1

A parameter study in a simplified geometry

Lampe, Nathanael; Karamitros, Mathieu; Breton, Vincent; Brown, Jeremy M.C.; Kyriakou, Ioanna; Sakata, Dousatsu; Sarramia, David; Incerti, Sébastien

DOI
10.1016/j.ejmp.2018.02.011

Publication date
2018

Document Version
Final published version

Published in
Physica Medica

Physica Medica 48 (2018) 135–145

Contents lists available at ScienceDirect

Physica Medica

journal homepage: www.elsevier.com/locate/ejmp

Original paper

Mechanistic DNA damage simulations in Geant4-DNA part 1: A parameter study in a simplified geometry

Nathanael Lampe[a,b], Mathieu Karamitros[b], Vincent Breton[a], Jeremy M.C. Brown[c], Ioanna Kyriakou[d], Dousatsu Sakata[b], David Sarramia[a], Sébastien Incerti[b,*]

[a] Université Clermont Auvergne, CNRS/IN2P3, Laboratoire de Physique Corpusculaire, F-63000 Clermont-Ferrand, France
[b] Université de Bordeaux, CNRS/IN2P3, CENBG, F-33175 Gradignan, France
[c] Radiation Science and Technology, Delft University of Technology, Mekelweg 15, Delft 26295B, The Netherlands
[d] Medical Physics Laboratory, University of Ioannina Medical School, Ioannina 45110, Greece

ARTICLE INFO

Keywords:
DNA damage
Geant4
Monte Carlo track structure

ABSTRACT

Mechanistic modelling of DNA damage in Monte Carlo simulations is highly sensitive to the parameters that define DNA damage. In this work, we use a simple testing geometry to investigate how different choices of physics models and damage model parameters can change the estimation of DNA damage in a mechanistic DNA damage simulation built in Geant4-DNA. The choice of physics model can lead to variations by up to a factor of two in the yield of physically induced strand breaks, and the parameters that determine scavenging, and physical and chemical single strand break induction can have even larger consequences. Using low energy electrons as primary particles, a variety of parameters are tested in this geometry in order to arrive at a parameter set consistent with past simulation studies. We find that the modelling of scavenging can play an important role in determining results, and speculate that high-scavenging regimes, where only chemical radicals within 1 nm of DNA are simulated, could provide a good means of testing mechanistic DNA simulations.

1. Introduction

Mechanistic modelling of radiation track structures in the cell nucleus allows researchers to test their understanding of the induction of cellular damage following ionising irradiation. Such simulations take a Monte Carlo track structure code and, beyond modelling the trajectory of particles defined by physical interactions, model the physico-chemistry that occurs in the radiolysis of water as well as the subsequent chemical reactions of radio-induced radicals. Currently, the two main codes which are used in these simulations are the PARTRAC platform [1] and the KURBUC code [2] (which represents developments that began based upon a geometric model devised by Charlton & Humm [3]). Both these codes have been used to investigate how ionising radiation and its products in water interact with geometrical models of DNA. In this work, we have used the Geant4-DNA track structure code [4,5], itself a part of the Geant4 Monte Carlo simulation toolkit [6–8], to model physics and radiochemistry in combination with a simple geometry that lets us assess the response of different parameters required for mechanistic track structure modelling. The aim of this work is to arrive at a consistent set of model parameters that replicate the assumptions of previous mechanistic simulation studies.

In medicine, radioprotection, space science and environmental radiobiology, understanding the action of ionising radiation is important for building a complete picture of how radiation affects living systems in both short term and long term contexts. In medicine, radiobiological simulations are frequently being sought after to improve the quality of treatment plans (for recent reviews of track structure codes in biophysical studies, see [9,10]), and the Geant4-DNA physics codes integrated into the TOPAS simulation platform [11] have recently been shown to replicate past microdosimetry studies [12]. In radioprotection, mechanistic simulations form an important part of understanding the magnitude of individual, rare ionisations, which is important at low doses where epidemiological studies are noisy, and the Linear-No Threshold model of dose effects may break down [13,14]. This is even more pronounced in chronic low dose studies, where ionising radiation may even act as a hormetic agent [15,16], or in understanding how chronic exposure to cosmic radiation by astronauts may impact health. Essentially, when doses are large, approximations made by microdosimetric models (e.g. the Local Effect Model, Microdosimetric Kinetic Model) are justified [17–19], but when doses are low, the impacts of ionising radiation are more difficult to discern, and can help elucidate how ionising radiation may be linked to eventual

* Corresponding author.
E-mail address: incerti@cenbg.in2p3.fr (S. Incerti).

https://doi.org/10.1016/j.ejmp.2018.02.011
Received 26 June 2017; Received in revised form 24 October 2017; Accepted 14 February 2018
Available online 05 April 2018

biological end points. Mechanistic DNA damage simulations represent an important step in building a 'bottom-up' picture of biological responses to ionising radiation.

An early parameter study of mechanistic DNA damage simulations was performed by Nikjoo et al. [20] (hereafter N97). In this study, straight DNA segments were positioned near electron track structures, and the physical and chemical DNA damage induced in the DNA was measured. This work laid a strong foundation for subsequent simulations with increased numbers of input particles and energies [21], and increasingly more realistic geometries [22]. Parallel development of the PARTRAC code [1,23–25] presents similar results, albeit with a different code. The differences between these platforms highlight that many assumptions need to be refined to better understand the processes that lead to DNA damage. This work presents a parameter study of DNA damage yields made using the Geant4-DNA platform in a geometry consisting of straight DNA segments placed with isotropic uniform randomness. Authors have already begun simulating cellular damage yields in Geant4-DNA [26], and thus a sensitivity study of the parameters that define DNA damage is needed to help understand these results. Furthermore, a set of parameters that is comparable between platforms is necessary to be able to clearly identify the strengths and weaknesses of each work, thus here we have attempted to find a parameter set that is justifiably comparable to those in N97.

In this work, we present our method, briefly describing our geometry and the approximations we have made to accelerate the simulation of chemistry. We next present our results, beginning with the impact of different physics models on yields of single strand breaks (SSBs) and double strand breaks (DSBs) in DNA, before exploring more in detail the implications of different parameters in the chemical phase of the simulation. We conclude the results with a brief investigation on whether it is valid to simulate only non-scavengeable radicals created close to DNA when considering cellular systems, due to the strong role played by DNA binding proteins in reducing scavenger abundances. In discussing and concluding our results, we highlight the necessity of building upon this parameter study with simulations of realistic cellular geometries.

2. Method

A test geometry, consisting of 200,000 rectangular boxes (100 × 30 × 30 nm), each containing a straight 216 bp segment of DNA, were placed in a 3 µm spherical volume (Fig. 1) using a previously described Geant4 application [27]. The position and orientation of each prism was randomly determined, and checks were made to ensure that prisms did not overlap. Primary electrons were created with random

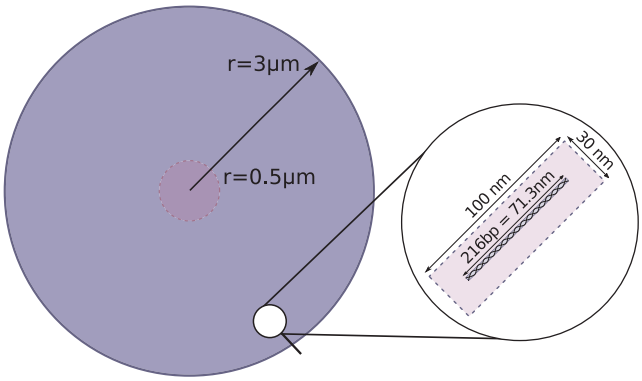

Fig. 1. The testing geometry consists of a 3 µm sphere filled with 200,000 individual 216 bp straight DNA segments in a rectangular placement volume. Primary electrons are generated randomly, with a random direction in a smaller 500 nm sphere in the centre of the test region. As the maximum primary energy is 4.5 keV, no primaries can escape the larger spherical region, and all primaries see an equivalently random spatial distribution of DNA segments.

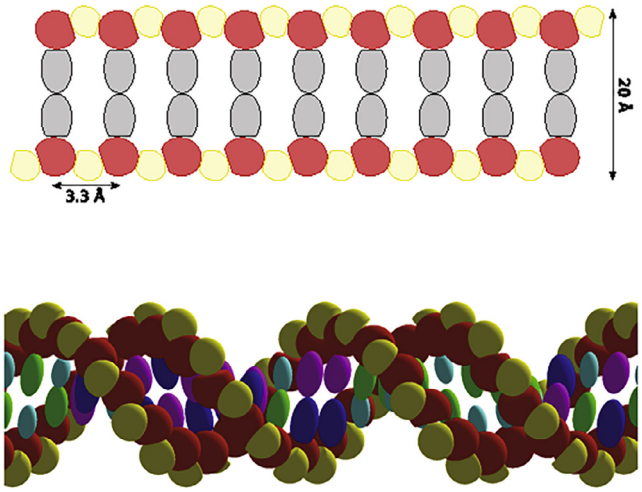

Fig. 2. Phosphate (yellow), deoxyribose (red) and base pairs (grey, top panel; other colours, bottom panel) are aligned and cut along one axis to be placed into the simulation without overlaps. The structure of the base pairs is shown schematically (top), and also rendered in Geant4 using openGL (bottom). (For interpretation of the references to colour in this figure legend, the reader is referred to the web version of this article.)

directions at random positions inside a radius 5 nm sphere at the center of this geometry, meaning each electron saw roughly isotropically placed DNA fibres. This is a different geometrical regime to the µ-randomness used by N97, however it serves well for investigating the impact of different model parameters on strand break yields, and fits better with the structure of our simulation code, which has been designed to allow many geometries to be simulated generically. As there is no large-scale order to the positions of DNA, the yields of strand breaks should not be compared to cellular DNA, but may be loosely compared to plasmid data, where there is less large scale geometrical order to the positions of DNA chains compared to cellular DNA.

Each 216 bp long DNA chain is composed of a repeating series of base pair molecules (guanine, adenine, cytosine and thymine), phosphate molecules, and deoxyribose molecules. These are rotated and cut along their z-axis inside Geant4 to avoid overlaps (Fig. 2). Chemical reactions are modelled between the bases, and the sugar molecules based on the reaction rates shown in Table 1. Chemically, we consider the deoxyribose and phosphate molecules together, with their position defined by the position of the deoxyribose molecule. All other chemical reaction rates, and radical diffusion properties, are unchanged from the Geant4-DNA default chemistry implementation [28,29], though an alternative time stepping method was used based on the Independent Reaction Times (IRT) model [30], which resulted in faster simulation of the chemical stage. We also introduced a variable parameter, r_{kill} in the chemical stage which defines a radius from the DNA chain beyond which chemistry would not be simulated. This avoids the need to simulate radicals that would not interact with DNA. Following N97, we stopped the chemical simulation after 1 ns, reflecting the typical scavenger densities in cellular media, and that radicals beyond 4 nm (the distance the ˙OH radical diffuses in 1 ns) from DNA are unlikely to

Table 1
Reaction rates used between radicals and DNA components ($\times 10^9$ L mol^{-1} s^{-1}), from Buxton et al. [65].

	˙OH	H˙	e^-_{aq}
$C_6H_5O_6P$	1.8	0.029	0.01
Adenine	6.1	0.10	9.0
Thymine	6.4	0.57	18.0
Guanine	9.2	–	14.0
Cytosine	6.1	0.092	13.0

induce chemical damage. We do highlight that our geometrical model (being composed of molecules rather than hemispheres) and our treatment of chemistry as chemical reactions with these molecules are pronounced deviations from N97. These changes manifest themselves in the strand break efficiency, and a higher proportion of SSBs that may occur due to indirect processes without energy being deposited in nearby DNA molecules.

Geant4-DNA offers three sets of alternative physics models for the simulation of electron interactions with liquid water. These sets ("default", "option 4" and "option 6"), have been described in detail in our previous publications [5,31–33]. Inelastic interactions (ionisation and excitation) are modelled in the default and option 4 sets using models based on the Emfietzoglou's parameterisation of the dielectric response function of liquid water. The default set has been recently improved in option 4 to provide a larger and more realistic excitation cross section data compared to data in the gas phase, as well as more accurate low energy corrections, particularly for exchange and correlation in electron-electron interactions. Option 6 however is a full porting of the well-known CPA100 track structure code, using the relativistic Binary-Encounter-Bethe approach for the modelling of ionisation and the Dingfelder model of the dielectric response of liquid water for excitation. To model elastic scattering, a partial wave approach is used for the default option, while the option 4 approach uses an improved screened Rutherford model with a screening factor obtained from vapour water data; option 6 adopts the classical Independent Atom Method. The default set also includes the modelling of attachment and vibrational excitation processes. Globally, option 4 is a significant improvement of Geant4-DNA physics models, allowing for more accurate simulations of W-values (the mean energy to create an ion pair) and dose point kernels [34]. Similarly, option 6 simulates much less diffusive dose point kernels compared to the default set [35]. This work investigates for the first time the influence of these model sets on DNA damage induction. When physical interactions only are simulated, these three sets apply by default a tracking cut-off below which the kinetic energy of electrons is locally deposited: 7.4 eV for the default set, 9 eV for option 4 and 11 eV for option 6. If the modelling of water radiolysis is activated, electrons are tracked down to thermalisation.

While we compare all three physics constructors, for the majority of simulations electron transport was simulated using the Geant4-DNA option 4 constructor [31], which provides more accurate cross-sections for electrons below 10 keV than the default constructor, and thus represents the best model for modelling DNA damage by low energy electrons. Both the medium and DNA molecules were composed of the same liquid water material (the Geant4-DNA models are based on electron transport within liquid water). We investigated the impact of different physics models on physically induced DNA damage, using the default, option 4, and option 6 [32] constructors (noting that the option 6 constructors is a modern implementation of the CPA100 models used by N97). Physically induced DNA damage was calculated based on three parameters, a radius r_{phys} from DNA molecules at which energy deposits would be considered to interact with DNA (Fig. 3), and lower E_{low} and upper E_{high} energy bounds for the energy deposit near a given

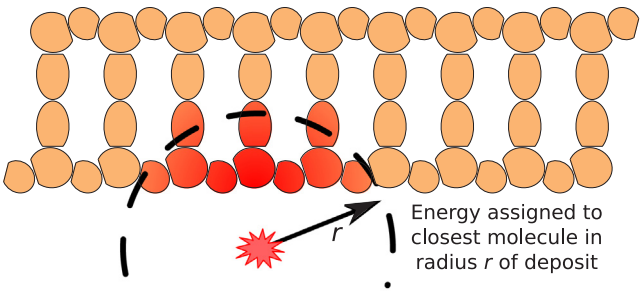

Fig. 3. Physical Damage attribution.

DNA molecule required to induce a strand break. An energy deposit within r_{phys} of either the deoxyribose or phosphate molecules belonging to a given base pair of DNA was considered to induce an SSB if the energy deposited exceeded E_{high}, and correspondingly, it was considered to induce no SSB if the energy deposit was less than E_{low}. Between these two values, SSBs were induced with a linearly varying probability. This criteria enabled us to simulate both the break criteria used by the PARTRAC [1] model (E_{low} = 5 eV, E_{high} = 37.5 eV), and the model used in N97 (E_{low} = E_{high} = 17.5 eV).

We classified DNA damage based upon the classification scheme of N97 (Fig. 4). This provides a classification of DNA damage by both complexity and source. We extend the scheme slightly by explicitly specifying its dependence upon two parameters, d_{DSB} and d_S, respectively the maximum distance between two SSBs on opposite sides of the DNA chain for the two nearby breaks to be considered a DSB, and d_S, the space between two damaged DNA segments for them to be considered independently. In this work, we consider d_{DSB} = 10 bp, and we consider each 216 bp long DNA segment independently from each other. Beyond the simple classifications, SSB+ refers to any number of breaks on only one side of the DNA strand, while 2SSB occurs when DNA is damaged on both sides of the chain, but the two damage sites are separated by more than d_{DSB}. DSB+ requires that the at least three damage events occur within d_{DSB}, with at least one on each strand, while DSB++ requires that at least two DSBs occur on the same damaged segment. When classifying damage by source, we consider both indirect, direct, mixed origin and hybrid DSBs. The differentiating factors between these classifications are that for a direct DSB (DSB_d), all DSBs on the segment must be from direct sources, for an indirect DSB (DSB_i), all DSBs on the segment considered must be from indirect sources, and for a mixed DSB (DSB_m), at least two DSBs occur, one which is indirect or hybrid, and the other which is direct. A hybrid DSB (DSB_{hyb}) occurs when a DSB would not occur but for the presence of indirect damage. Typically, we consider DSB_m and DSB_h together, following N97, noting that DSB_m dominates DSB_{hyb}.

Whilst across the simulations we conduct many parameters are varied, this is done largely from a set of parameters which best represents the work conducted by N97 (Table 2). We introduce here the parameter p_{SSB} which refers to the likelihood that an SSB is induced following a chemical reaction between a sugar-phosphate moiety and a radical (typically $^{\cdot}$OH). Previous experimental work shows that not all reactions between DNA and $^{\cdot}$OH result in strand breaks [36,37], and this parameter is used to establish the correct efficiency of strand break formation following these reactions. We note that these parameters were not chosen to make our data fit the results of N97, but rather to provide the same starting point for comparison between our simulation results and what is established in the literature.

In the following sections, we explore the effects of varying the physics list chosen, E_{low}, E_{high} and r_{phys} on the yields of SSBs and DSBs from physics processes alone. For each scenario considered here, 1 GeV of energy deposition was simulated, with primary electrons having either energies of 300 eV, 500 eV, 1 keV, 3 keV and 4.5 keV in each run. These energies were chosen because of their importance in water radiolysis, as the sources of spurs, blobs and short tracks [38]. Then, using 4.5 keV electrons and a total energy deposit of 1.5 GeV (333,333 primaries), we consider how setting a 1 ns end time on the chemical component of the simulation impacts the chemical reactions that can occur, alongside how different values of r_{kill} impact the yields of strand breaks. For these initial chemical simulations, p_{SSB} was set to 0.65, similar to Kreipl et al.'s value of p_{SSB} = 0.7 [24], and Nikjoo et al.'s implicit value of p_{SSB} = 0.65 [20]. We then considered more broadly the role of the parameter p_{SSB} in determining the efficiency chemically induced strand break formation, to find which value best replicates the assumptions made in N97, so accordingly we then compare our simulations to those in N97, alongside some experimental results in plasmids. For each of the primary electron energies we consider here (300 eV, 500 eV, 1 keV, 3 keV and 4.5 keV), the number of primaries

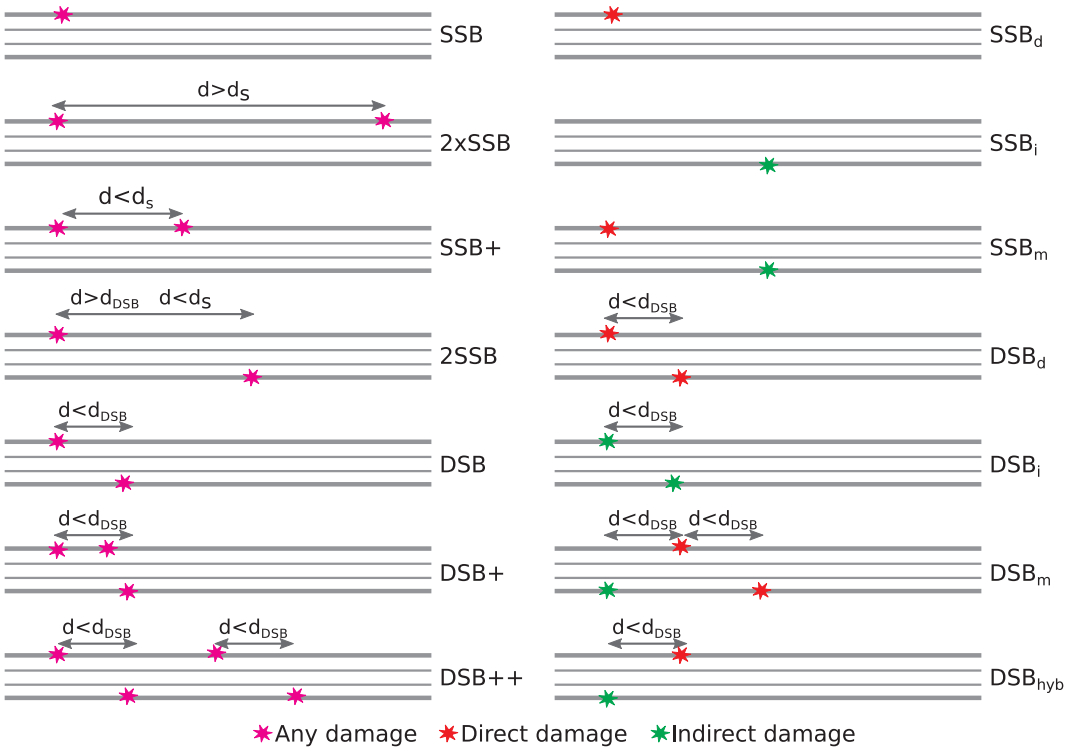

Fig. 4. DNA damage is classified according to the scheme originally proposed by N97 (discussed in text).

Table 2
Simulation parameters that best match N97.

Parameter	Description	Value
E_{low}	Lower limit for physical damage	17.5 eV
E_{high}	Upper limit for physical damage	17.5 eV
r_{phys}	Radius for direct damage	6 Å
d_{DSB}	Distance between SSBs for DSB	10 bp
r_{kill}	Distance from DNA to kill radicals	4 nm
p_{SSB}	Pr(˙OH + $C_6H_5O_6P \rightarrow$ SSB)	0.4
–	Simulation End Time	1 ns
–	Max. IRT time step	500 ps

simulated is chosen to yield 1 GeV of deposited energy in total.

3. Results

We begin by exploring the parameters that affect the physical stage of the simulation. Fig. 5 illustrates the effect that different physics models and damage models can have on SSB and DSB yields, due to the differing cross-section calculations used in each model. For each given physics model, more damage is always measured by the PARTRAC damage model (5–37.5 eV) than the N97 model (17.5 eV). The likelihood of a SSB or DSB occurring is closely related to the magnitude of the interaction cross-sections in each model, which are highest in the CPA100 models (Geant4-DNA option 6), causing this model to show the

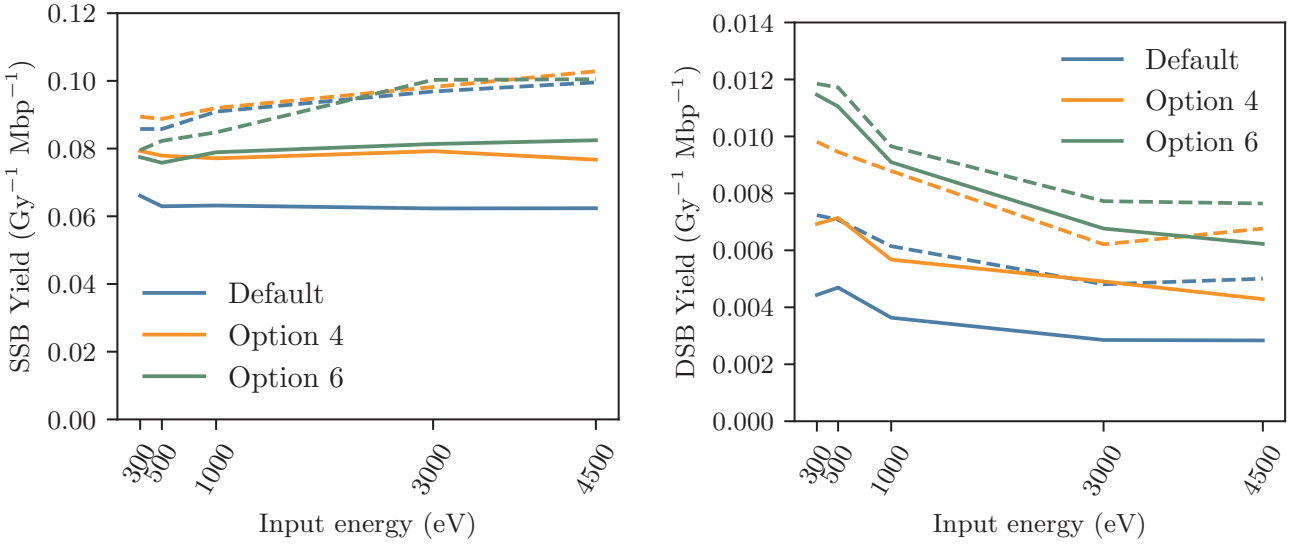

Fig. 5. Different physics models can have a large impact on SSB and DSB yields. We also show the impact of using 17.5 eV (straight) and 5–37.5 eV (dotted) energy thresholds for physical damage induction.

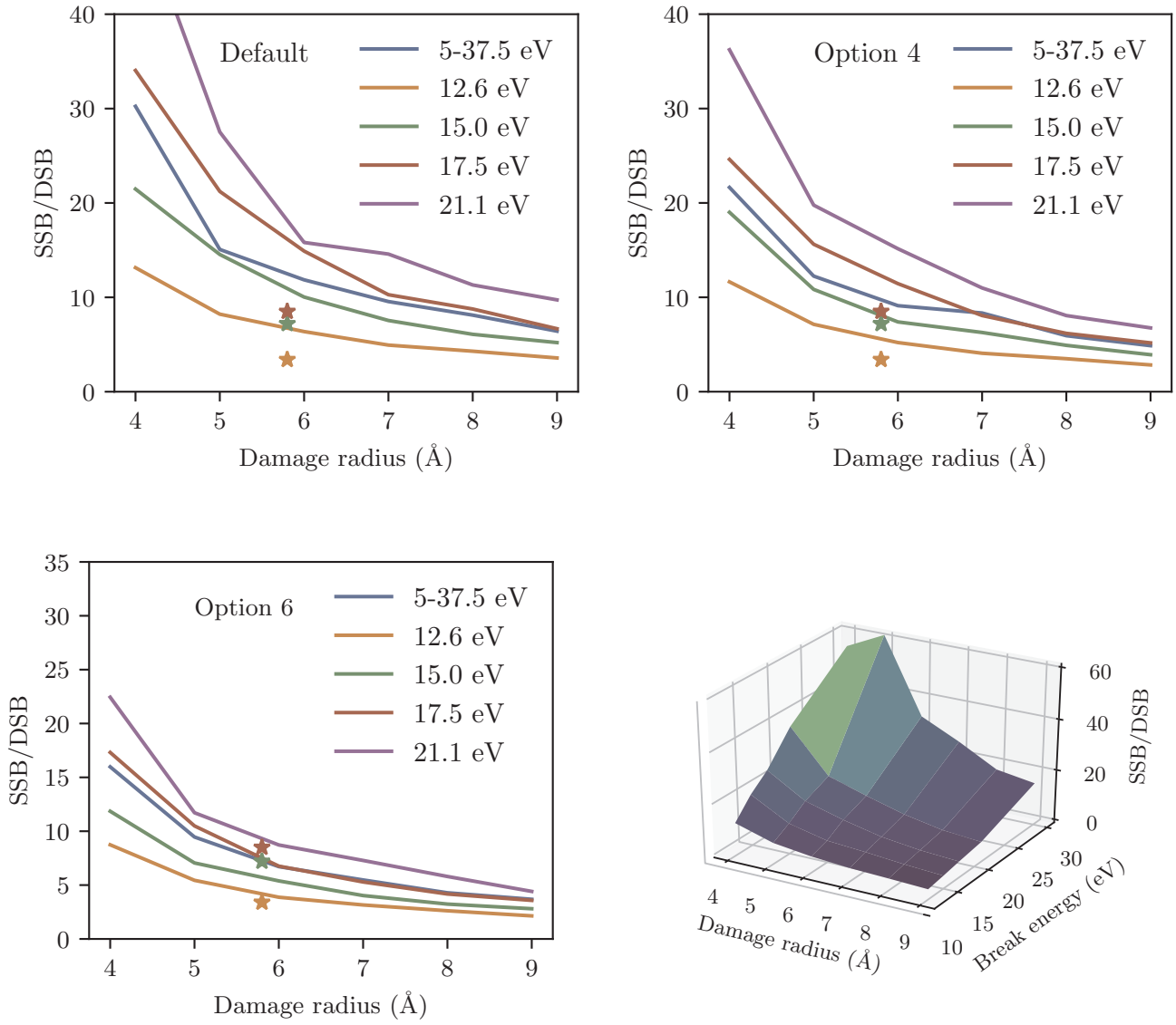

Fig. 6. Varying the break induction thresholds, damage radius (r_{phys}) and physics model all impact the ratio of SSBs to DSBs, which behaves approximately as the reciprocal of the probability of inducing a break. For each model considered, we plot the SSB to DSB ratio measured in N97 for physical damage at an equivalent damage radius. The inverse relationship between the break induction radius, and energy threshold is shown in the bottom right panel, for option 4.

highest SSB and DSB yields [4]. Compared to a previous Geant4-DNA based physics study using the default model, and taking $E_{low} = E_{high} = 10.79$ eV [39], SSB and DSB yields estimated using the PARTRAC damage model reproduce this work well.

It should be noted that the inelastic model implemented in option 4 has been further improved by Emfietzoglou and co-workers [40], based on more recent experimental data for the dielectric response function of liquid water [41,42]. The new model exhibits more pronounced broadening effects in the energy loss function which, along with its shifting to lower losses, is expected to further exaggerate the differences with the inelastic cross sections of the default model, especially below a few hundred electron-volts [43]. It has been recently shown that such differences in the dielectric function have a strong impact on energy deposition in targets of nanometer size [44,45]. The impact of these changes upon our results would be an interesting avenue for further study.

Across all physics models considered, r_{phys} and the energy threshold required for a break are inversely related, as shown in the dependence of the ratio of SSBs to DSBs as these parameters vary (Fig. 6), which drops as breaks become easier to induce. The PARTRAC break model behaves similarly to a constant break induction energy between 15 eV and 17.5 eV for the physics models considered. Option 4 and option 6 both reproduce certain SSB/DSB ratios measured by N97 (considering a radius from the DNA molecule that gives a similar volume to the N97 DNA model). This is expected for the option 6 physics models, which are a modern implementation of the CPA100 models used by N97, while the agreement between N97 and the option 4 models at 15 eV is more coincidental, and the difference between the models is shown in the large change in the SSB/DSB ratio that occurs when passing from a 15 eV threshold to a 17.5 eV threshold. Physics models also impact the distribution of break complexities (Fig. 7), with each model being in reasonable agreement with N97. Slight changes from N97 include the default and option 4 Geant4-DNA models favouring simple rather than complex damage than N97, whilst option 6 favours more complex breaks than N97 suggests.

In the absence of any simulation end time, radicals diffuse and react with DNA until all radicals have disappeared (Fig. 8 left). Such a simulation effectively considers DNA to be the only 'scavenger' in the medium, and, as radicals further and further from the DNA chain are considered (by increasing r_{kill}), they diffuse and react with DNA. Following N97, we stop the simulation of chemistry after 1 ns (Fig. 8 right), which means that over 95% of ˙OH radicals that react with DNA

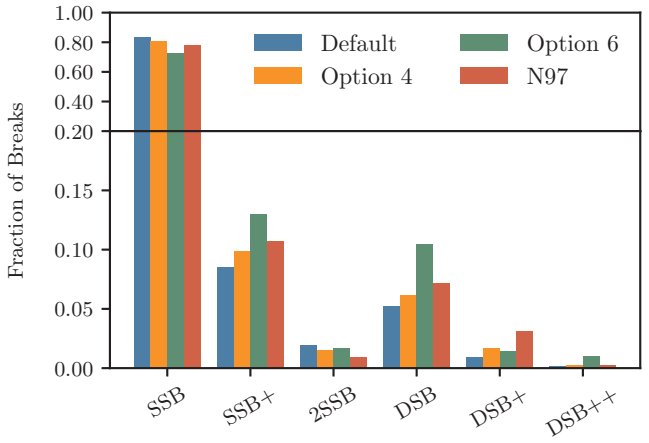

Fig. 7. Break complexities yielded for physical damage from 300 eV electrons using different physics models. Here we consider the percentage of breaks falling into each complexity case considered, alongside the complexity distribution for physical damage only from N97. The scale is broken to better indicate the differences in the rarer DSB classifications.

only are created within and remain inside the 4 nm of water surrounding the DNA chain. Due to its higher diffusivity, about 20% of the reactions between e^-_{aq} and DNA are effectively hidden when only simulating chemistry within 4 nm of DNA, however this doesn't impact the results reported in this work, as e^-_{aq} is not thought to be a major contributor to strand breaks, as it primarily reacts with the DNA bases. Further experimental investigation ought to be conducted to determine with what efficiency reactions between bases from aqueous electrons and other radicals can induce SSBs, as authors have shown resonances induced in the outer orbitals of DNA bases can cause SSBs [46]. When considering the strand breaks these chemical reactions induce (Fig. 9), we see that as r_{kill} increases, the number of indirect breaks increases, with indirect SSBs reaching a plateau near $r_{\text{kill}} = 6$ nm and the indirect DSBs reaching a plateau near $r_{\text{kill}} = 4$ nm. Throughout this range, directly induced breaks are converted to mixed breaks, with a large portion of this conversion coming from the conversion of SSB_d to DSB_m and DSB_hyb.

As a free parameter, p_{SSB} can be used to limit the amount of indirect damage that occurs, so that simulations match experiments, however bounds can be placed on it based upon the efficiency with which ˙OH interacts with DNA. Based upon the reaction rates we have chosen, 68% of ˙OH radicals that react with DNA react with base molecules, while the rest react with strand molecules. This can be deduced from Fig. 10, where 32% of all reactions between ˙OH and DNA cause an SSB when $p_{\text{SSB}} = 1$. N97 follow the measurement of Milligan et al. [36], who measure that 12% of all reactions between ˙OH and DNA cause an SSB, suggesting that $p_{\text{SSB}} = 0.4$ is an appropriate value for our system. There is however large scope for p_{SSB} to vary, with other authors suggesting different efficiencies for strand break formation [37], and certain measurements indicating our reaction rates lead to an incorrect ratio of reactions between ˙OH and bases and strands, which may be closer to 80:20 [47].

Examining each parameter individually, the set of parameters in Table 2 provides a best match of the system modelled by N97. Under these conditions, our model finds notably more indirect damage than N97. This is seen first in Table 3, where we show the fraction of DNA subjected to some form of DNA damage which have had either no energy, 0^+–60 eV, 60–150 eV or > 150 eV of energy deposited in them. A significant number of segments are damaged indirectly, but have no energy deposited inside them physically. These were excluded from the normalisation in Table 3 to better mimic what N97 produces. The breakdown of energies deposited in DNA matches well with that found by N97, however when we consider the DSBs induced by different energy depositions, the higher amount of indirect damage that we report leads us to suggest that it is deposits of 0^+–60 eV in DNA that are the dominant cause of DSBs rather than the more energetic deposits of 60–150 eV reported by N97. Across all the energies we considered, almost 20% of DSBs are induced by radical diffusion, with no physical energy being deposited at all in the DNA segment.

The yields of SSBs and DSBs by complexity and source are given in Tables 4 and 5 respectively. Geant4-DNA finds higher total damage yields, though in the absence of a cell geometry, it is difficult to compare how much of this is due to the differences between the isotropic randomness we have selected for testing purposes, and the μ-randomness used by N97. For 300 eV and 4500 eV electrons, we see that after the addition of chemistry, Geant4-DNA comparatively favours simple rather than complex damage in comparison to N97 (Fig. 11). When comparing damage sources, indirect damage dominates direct damage in Geant4-DNA, with around 80% of SSB events across all energies coming from chemical sources. While this disagreement is severe, our work is in line with both the PARTRAC simulation platform's predictions [23] and experimental measurements [48] of the contribution of indirect action to low LET radiation damage.

One way to force a better agreement with N97's high direct damage yields is to only simulate electrons within 1 nm of the DNA strand, motivated roughly by observations that in cellular and high-scavenging contexts, only non-scavengeable radicals created within the hydration shells of DNA cause indirect damage [49]. Conducting such a

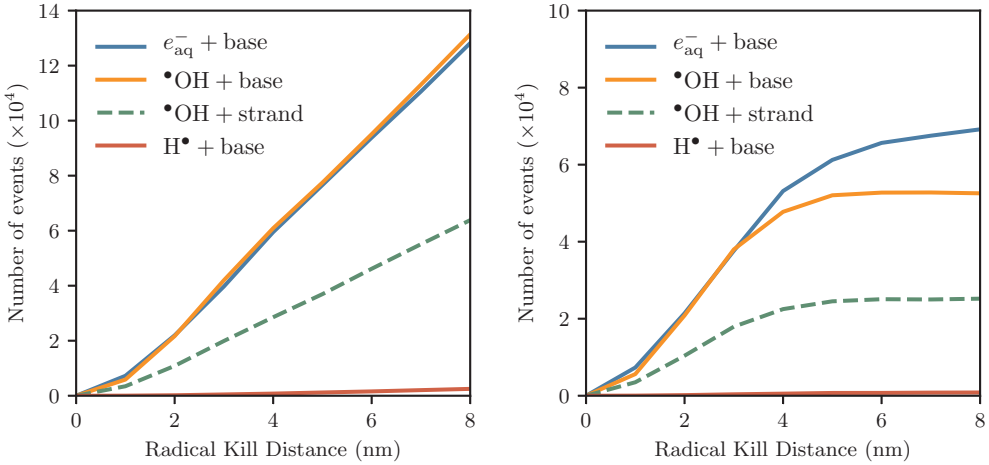

Fig. 8. The number of chemical reactions that occur when 333,333 primary 4.5 keV electrons interact with the geometry without (left) and with (right) a 1 ns simulation end time.

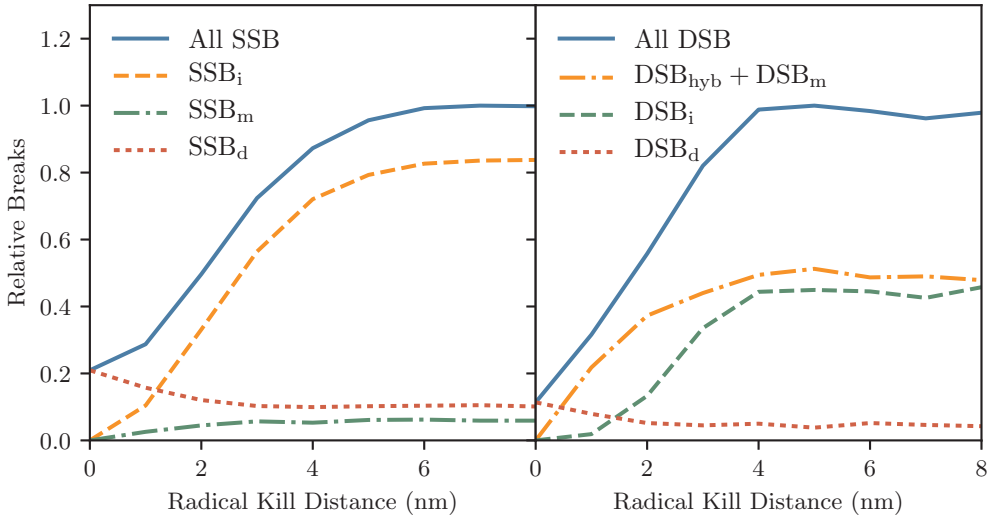

Fig. 9. The number of breaks by source changes as chemistry is simulated further from the DNA. Far from DNA, more indirect damage is induced, and in addition to pure indirect breaks, both direct SSBs and DSBs are converted to mixed damage.

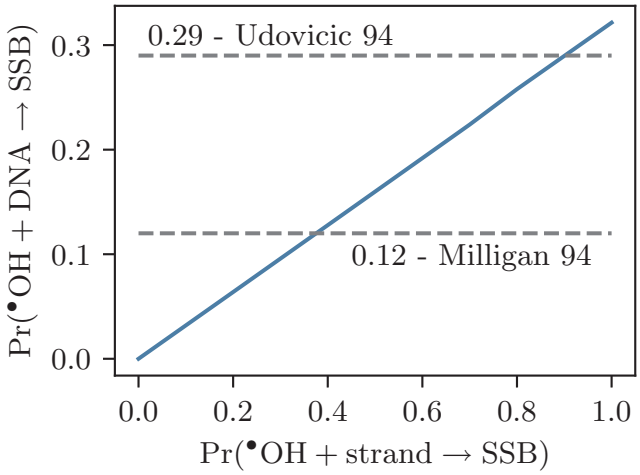

Fig. 10. The efficiency with which reactions between ˙OH and DNA strand reactions are converted into SSBs is a free parameter in our simulations. It can be compared to a conversion efficiency for all reactions between ˙OH and DNA, and compared to experimental data. Following N97, we seek to replicate the efficiency of Milligan et al. [36] rather than Udovicic et al. [37], and thus set $p_{SSB} = 0.4$.

simulation noticeably improves our agreement with N97 for the fraction of DSBs induced for a given energy deposit (Table 3, underlined values). For 4.5 keV electrons (Fig. 12), the results are in line with strand break yields from 4.55 keV X-rays [50] as well as measurements in plasmids where scavenging is extremely high [51]. We do note here that this agreement may be coincidental, as it occurs slightly beyond the 3rd DNA hydration shell (which ends 6.5 Å from the DNA chain [52]) and that while this geometry may bear some resemblance to the randomness found in grouped plasmids, it was conceived primarily to better understand the dynamics of mechanistic DNA damage simulations with Geant4-DNA.

4. Discussion

This study aims to understand how the many parameters that are necessary to mechanistically model DNA damage interact in a manner that is largely agnostic towards experimental results. We have attempted to find parameters that match those already well established in an existing work, whilst avoiding any result that may encourage us to 'fit' our parameters to a result. We need to mention that in doing so, we have implicitly adopted parameters fitted from other models, such as the 17.5 eV threshold for a physically induced strand break [3], when it is well known that very low energy electrons (5–10 eV) can interact with DNA to produce strand breaks [53]. While the large variation in strand break induction from physics models alone highlights what is perhaps the necessity to have free parameters that ensure a correspondence between simulations and biological data, from another perspective this prevents biological measurements from serving as a tool that validates the simulation chain, thus eroding our confidence that such simulations can be truly predictive.

The physical damage models of N97 and PARTRAC typically disagree for physically induced SSB and DSB yields at around the 20% level. In addition, the physics modelling in each simulation differs, with PARTRAC modelling the dielectric response of liquid water following Dingfelder et al.'s approach [54,55]. This contribution, compounded

Table 3
Frequency of energy depositions and DSBs in cells by primary electron energy (italicized values are from N97, underlined values are calculated with $r_{kill} = 1$ nm).

Energy	E_{dep} Frequency				DSB Frequency			
	0 eV	0^+–60 eV	60–150 eV	> 150 eV	0 eV	0^+–60 eV	60–150 eV	> 150 eV
300 eV	607.5	85.9	13.7	0.4	18.9	47.1	32.4	1.6
"	–	86	13	1	–	21	74	5
500 eV	523.8	86.2	13.3	0.5	19.1	49.1	30	1.8
1000 eV	463.3	88.6	10.9	0.5	19.8	48.5	29.3	2.3
3000 eV	497.3	93	6.8	0.2	21.3	53.7	23.7	1.3
4500 eV	516	93.6	6.1	0.2	20.6	53.9	23.4	2
"	–	92	7	1	–	30	64	16
"	56.6	91.8	7.9	0.5	0.4	44.5	51.0	4.1

Table 4
Breakdown of DSBs by complexity, using a parameter set that emulates N97.

Energy eV	None %	SSB %	SSB+ %	2SSB %	DSB %	DSB+ %	DSB++ %	$DSB_{complex}$ %	Hits –	Y_{SSB} $Gy^{-1}\,Mbp^{-1}$	Y_{DSB} $Gy^{-1}\,Mbp^{-1}$
300	82.41	12.59	2.07	0.68	1.56	0.38	0.31	30.46	105,792	0.265	0.039
500	80.73	13.53	2.23	0.96	1.8	0.38	0.37	29.39	90,105	0.245	0.037
1000	80.24	14.22	2.24	0.92	1.68	0.33	0.36	29.11	90,236	0.256	0.035
3000	82.69	13.51	1.56	0.62	1.22	0.22	0.19	24.92	115,684	0.296	0.031
4500	83.97	12.8	1.33	0.53	1.06	0.18	0.13	22.51	127,151	0.304	0.028

Table 5
Breakdown of breaks by source, using a parameter set that emulates N97.

Energy eV	SSB_i %	SSB_d %	SSB_m %	DSB_d %	DSB_i %	$DSB_{m/hyb}$ %	N_{SSB} –	N_{DSB} –
300	76.9	14.7	8.4	9.9	36.8	53.3	16,229	2380
500	76.7	14.7	8.6	9.4	37.6	53	15,060	2300
1000	76.5	15.2	8.4	8.6	37.7	53.7	15,692	2140
3000	78.2	15.6	6.2	7.9	40.7	51.4	18,152	1874
4500	78.7	15.5	5.8	8.3	39.3	52.4	18,639	1737

with the differences in physics models, indicates that our final predictions of SSB and DSB yields are approximate. When working in Geant4-DNA, both models ought to be considered to some extent, as there is no consensus as to which is correct, and both authors advance strong arguments in favour of their particular model [1,2]. Amongst the physics models studied, options 4 and 6 provide the best agreement with the SSB/DSB ratios measured by N97. Option 6, a modern, revised implementation of the CPA100 models that N97 use are derived from modelling electron impact ionisation via the Binary Encounter Bethe model [32], shows a better agreement with the measurements of N97

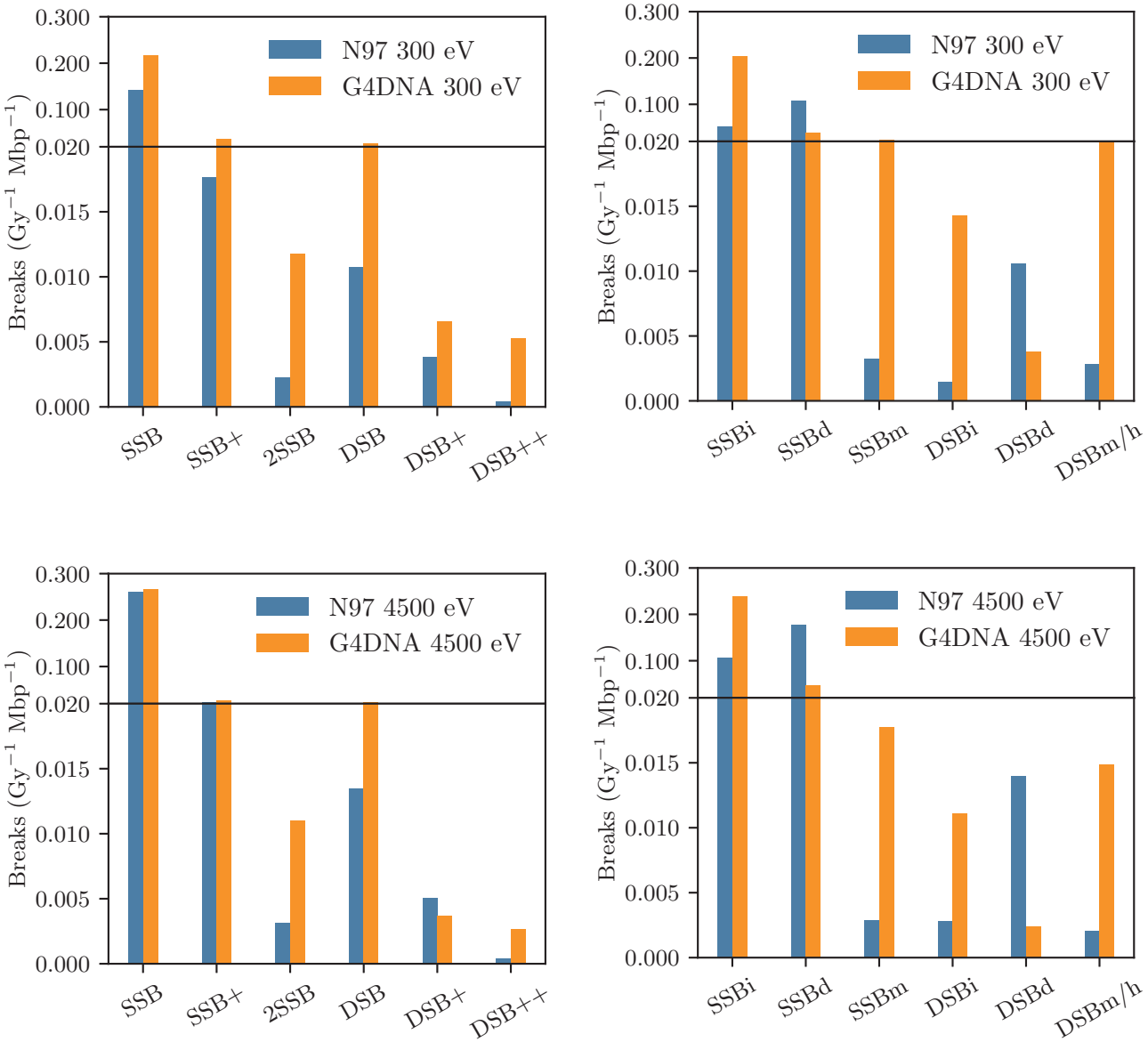

Fig. 11. Comparison of break complexity and source between Geant4-DNA option 4 and N97 for 300 eV and 4.5 keV electrons.

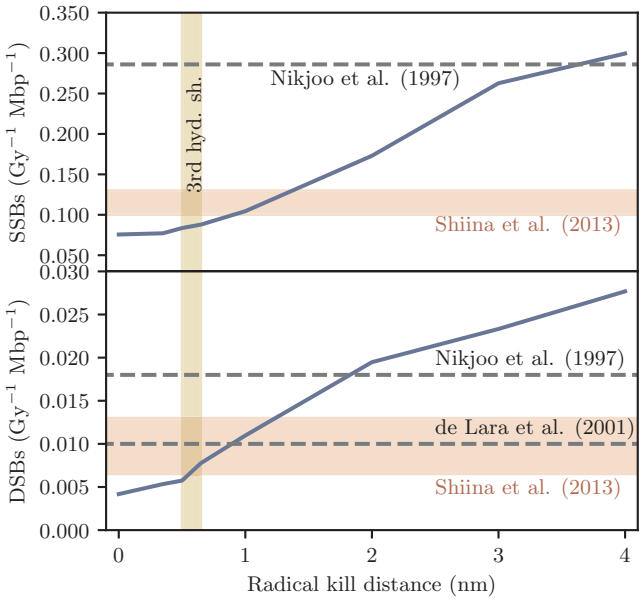

Fig. 12. Variation in DSB and SSB yields for 4.5 keV primary electrons for different values of r_{kill}. The radius of the 3rd hydration shell of DNA is highlighted as well as cellular DSB yields from de Lara et al. [50] from ultrasoft (4.55 keV) X-rays and plasmid DSB and SSB yields in a very high scavenging regime (Shiina et al. [51]) under X-irradiation. The yields of SSBs and DSBs from N97 are also plotted.

than option 4, which agrees well at a 15 eV break threshold, but poorly at 17.5 eV. Option 4 [56] is based on the dielectric model of liquid water [57], with an improved calculation of cross sections for electrons below 10 keV than the default models [31]. We have adopted option 4 for most simulations here as it reflects a more modern approach to track structure modelling, though properly determining the correct code requires significant progress to be made measuring electron cross-sections in liquid water. The significant increase in SSB/DSB in the option 4 models between a break threshold of 15 eV and 17.5 eV presents one way in which our model may miscalculate physical damage (Fig. 6). Despite this, option 4 presents a better agreement than option 6 with the complexities of damage found by N97, likely due to changes in the CPA100 code made over the last 20 years (Fig. 7).

The introduction of a 1 ns end time to the simulation is necessary to provide some measure of the scavenging which is present in nearly all cellular systems. In this time, ˙OH molecules diffuse a mean squared distance of 4 nm, seen in the drop off in ˙OH reactions that occurs when r_{kill} = 4 nm. Based on typical scavenger densities in cells, the ˙OH ought to diffuse 6 nm [58], better corresponding to the simulation end time of 2.5 ns used by other authors [1,26], though these simulations also simulate scavenging by structural proteins and chemical reactions, which is likely compensated for by the shortened simulation time. By varying r_{kill} it is possible to see the action of radiolysis in creating complex damage from damage that is otherwise simple in the chemical stage, where simple direct damage becomes complex mixed and hybrid damage as more chemistry is simulated (Fig. 9).

The efficiency with which indirect strand damage is converted to SSBs can act to drastically change the simulation result, and we have attempted to show that our choice of p_{SSB} = 0.4 is well motivated. Previous estimates of this parameter include p_{SSB} = 0.65 (from N97), p_{SSB} = 0.7 [24], and p_{SSB} = 0.42 [26]. The estimates near 0.65 seem to derive from a measured efficiency of SSB formation Pr(˙OH + DNA → SSB) = 0.12 [36], in combination with the measurement that ˙OH-Strand reactions compose 20% of all ˙OH-DNA reactions [47]. The estimate that p_{SSB} = 0.42, itself made in a simulation built from Geant4-DNA, is motivated though by the assumption that in DNA, only two of the five reaction sites of free deoxyribose are blocked in DNA, a strange conclusion given that all reaction sites of deoxyribose are observed to react with ˙OH, albeit with varying efficiencies [59]. The straight line plotted (from data) in Fig. 10 owes its form to the reaction rates that we have used, which lead to 32% of all ˙OH-DNA reactions to occur between the strand and the base. To reproduce the break efficiencies followed by N97 then, a value of p_{SSB} = 0.4 is required. We have chosen to match the break efficiency of Milligan et al. not only to follow N97, but also because in this work, a reaction rate between ˙OH and DNA of 2.7×10^9 L mol^{-1} s^{-1} is found, which is of a similar order of magnitude to the reaction rates we consider for the individual DNA components. An alternative work [37] suggests an overall efficiency of 29% is more correct, however this also predicts a very low reaction rate between ˙OH and DNA (4.6×10^8 L mol^{-1} s^{-1}). A possible extension of this study could examine the role of varying the reaction rates between ˙OH and DNA molecules, though grounding this study in experimentally feasible ranges is important.

Quite remarkable in our comparison with N97 is the very different predictions we make for indirectly induced damage (Fig. 11). Even in more recent works, predictions built on the N97 model [21] indicate that direct damage dominates indirect DNA damage. Our simulations however show that indirect effects dominate direct effects, in agreement with predictions from the PARTRAC [23,60] and previous work in Geant4-DNA [26]. The role of indirect action is experimentally quantified by measuring DNA damage with different abundancies of radical scavengers, or by measuring damage in wet and dry plasmids where radicals created in water can increase DNA damage by two or three times [49]. High concentrations of the scavenger DMSO can protect cells from up to 80% of damage that would otherwise be induced, with only unscavengeable radicals created in the hydration shells of DNA being capable of inducing damage. Our simulation lets us simulate only the effects of these radicals on DNA by using very small values of r_{kill}. This condition, which stops nearly 60% of DNA damage for 4.5 keV electrons, is considered in Fig. 12. Additionally, it changes the balance of induced damage so that physically induced SSBs dominate SSBs induced by chemical processes. While further investigation is necessary, particularly in cellular geometries, the simulation of damage caused only by radicals close to the hydration shell could be one way to improve the realism of mechanistic DNA damage simulations. We show that our results for unscavengeable damage, envisaged as radicals created less than 1 nm from DNA, agree well with measurements of DNA damage in cells submitted to 4.55 keV X-irradiation [50] and in plasmids [51] exposed to 4 keV µm^{-1} X-rays, though the appropriateness of a comparison between our simulations and these experiments is not necessarily accurate, given the differences in the DNA geometry simulated. It should be stressed though that our comparisons to measurements in cells are biased by the non-realistic testing geometry used here, and that the range of biological processes that occur in cells to repair DNA introduce a complexity in the measurements that is not included in simulation.

All our comparisons to other works made in this study are hampered by the geometry we have used being different to other works. Our geometry was chosen to enable the important parameters in our models to be studied, so that they may be understood independent of a realistic cellular geometry. The use of many short DNA strands, rather than µ-randomness [61], or a realistic geometry likely inflates our estimation of DSB yield relative to cells, as our geometry has no large-scale order, and cutting DNA into 216-bp long pieces increases the number of interactions a given particle track will have with DNA segments. This represents far more what is observed in plasmids, which keep some aspects of a random packing, rather than cells, in which folding proteins give some large range order to the conformity of DNA. The logical extension of this work is to take this model and see how it performs in a full cellular geometry. To this end, we present in an accompanying paper DNA damage simulations in a model of a bacterial *Escherichia coli* cell [62] as part of a larger project to quantify the impact of the natural radiation background on a bacterial system [63].

5. Conclusion

We have presented in this work the results of many simulations that explore the parameters that can define the induction of SSBs and DSBs in mechanistic DNA damage simulations. Rather than conduct a fit to experimental data, we have tried to identify why each of the parameters we have used is comparable to those from N97. Interestingly, Geant4-DNA predicts under these parameters that most radio-induced biological damage comes from indirect sources, in agreement with the predictions of PARTRAC, and in conflict with N97.

As we have used a model geometry in this study, comparison to biological data is limited, and while we do not expect the trends observed here to change when passing to a more realistic geometric model, the normalisation parameters may. We are currently developing a geometric model of an *E. coli* bacterium to be better able to compare our results to biological data, and future work may extend this work to more complex cells.

We conclude by highlighting the importance of this work to DNA damage simulations conducted not only in Geant4-DNA, but also in the toolkits that inherit Geant4-DNA models such as TOPAS and GATE [64]. As these platforms rely on the same underlying physics and chemical models, the variations between physics models we observe here will propagate to these simulation toolkits also.

References

[1] Friedland W, Dingfelder M, Kundrát P, Jacob P. Track structures, DNA targets and radiation effects in the biophysical Monte Carlo simulation code PARTRAC. Mutat Res 2011;711:28–40. http://dx.doi.org/10.1016/j.mrfmmm.2011.01.003. Elsevier B.V.

[2] Nikjoo H, Emfietzoglou D, Liamsuwan T, Taleei R, Liljequist D, Uehara S. Radiation track, DNA damage and response—a review. Rep Prog Phys 2016;79:116601. http://dx.doi.org/10.1088/0034-4885/79/11/116601. IOP Publishing.

[3] Charlton DE, Humm JL. A method of calculating initial DNA strand breakage following the decay of incorporated 125I. Int J Radiat Biol 1988;53:353–65. http://dx.doi.org/10.1080/09553008814552501.

[4] Bernal MA, Bordage MC, Brown JMC, Davídková M, Delage E, El Bitar Z, et al. Track structure modeling in liquid water: a review of the Geant4-DNA very low energy extension of the Geant4 Monte Carlo simulation toolkit. Phys Medica 2015:1–14. http://dx.doi.org/10.1016/j.ejmp.2015.10.087.

[5] Incerti S, Ivanchenko A, Karamitros M, Mantero A, Moretto P, Tran HN, et al. Comparison of GEANT4 very low energy cross section models with experimental data in water. Med Phys 2010;37:4692–708. http://dx.doi.org/10.1118/1.3476457.

[6] Allison J, Amako K, Apostolakis J, Arce P, Asai M, Aso T, et al. Recent developments in Geant4. Nucl Instr Methods Phys Res Sect A 2016;835:186–225. http://dx.doi.org/10.1016/j.nima.2016.06.125.

[7] Allison J, Amako K, Apostolakis J, Araujo H, Arce Dubois P, Asai M, et al. Geant4 developments and applications. IEEE Trans Nucl Sci 2006;53:270–8. http://dx.doi.org/10.1109/TNS.2006.869826. IEEE.

[8] Agostinelli S, Allison J, Amako K, Apostolakis J, Araujo H, Arce P, et al. GEANT4 – a simulation toolkit. Nucl Instr Methods Phys Res Sect A 2003;506:250–303. http://dx.doi.org/10.1016/S0168-9002(03)01368-8. Detect Assoc Equip.

[9] Nikjoo H, Uehara S, Emfietzoglou D, Cucinotta FA. Track-structure codes in radiation research. Radiat Meas 2006;41:1052–74. http://dx.doi.org/10.1016/j.radmeas.2006.02.001.

[10] El Naqa I, Pater P, Seuntjens J. Monte Carlo role in radiobiological modelling of radiotherapy outcomes. Phys Med Biol 2012;57:R75–97. http://dx.doi.org/10.1088/0031-9155/57/11/R75.

[11] Perl J, Shin J, Schümann J, Faddegon B, Paganetti H. TOPAS: an innovative proton Monte Carlo platform for research and clinical applications. Med Phys 2012;39:6818. http://dx.doi.org/10.1118/1.4758060.

[12] McNamara AL, Geng C, Turner R, Ramos-Méndez J, Perl J, Held K, et al. Validation of the radiobiology toolkit TOPAS-nBio in simple DNA geometries. Phys Medica 2016;33:207–15. http://dx.doi.org/10.1016/j.ejmp.2016.12.010. Associazione Italiana di Fisica Medica.

[13] Tubiana M, Feinendegen LE, Yang C, Kaminski JM. The linear no-threshold relationship is inconsistent with radiation biologic and experimental data. Radiology 2009;251. http://dx.doi.org/10.1148/radiol.2511080671.

[14] Little MP, Wakeford R, Tawn EJ, Bouffler SD, Berrington de Gonzalez A. Risks associated with low doses and low dose rates of ionizing radiation: why linearity may be (almost) the best we can do. Radiology 2009;251:6–12. http://dx.doi.org/10.1148/radiol.2511081686.

[15] Castillo H, Schoderbek D, Dulal S, Escobar G, Wood J, Nelson R, et al. Stress induction in the bacteria *Shewanella oneidensis* and *Deinococcus radiodurans* in response to below-background ionizing radiation. Int J Radiat Biol 2015;3002:1–33. http://dx.doi.org/10.3109/09553002.2015.1062571.

[16] Calabrese EJ. Hormetic mechanisms. Crit Rev Toxicol 2013;43:580–606. http://dx.doi.org/10.3109/10408444.2013.808172.

[17] Elsässer T, Krämer M, Scholz M. Accuracy of the local effect model for the prediction of biologic effects of carbon ion beams in vitro and in vivo. Int J Radiat Oncol Biol Phys 2008;71:866–72. http://dx.doi.org/10.1016/j.ijrobp.2008.02.037.

[18] Brown JMC, Currell FJ. A local effect model-based interpolation framework for experimental nanoparticle radiosensitisation data. Cancer Nanotechnol 2017;8:1. http://dx.doi.org/10.1186/s12645-016-0025-6. Springer Vienna.

[19] Hawkins RB. A microdosimetric-kinetic model for the effect of non-Poisson distribution of lethal lesions on the variation of RBE with LET. Radiat Res 2003;160:61–9. http://dx.doi.org/10.1667/RR3010.

[20] Nikjoo H, O'Neill O, Goodhead T, Terrissol M. Computational modelling of low-energy electron-induced DNA damage by early physical and chemical events. Int J Radiat Biol 1997;71:467–83.

[21] Nikjoo H, O'Neill P, Wilson WE, Goodhead DT. Computational approach for determining the spectrum of DNA damage induced by ionizing radiation. Radiat Res 2001;156:577–83. http://dx.doi.org/10.1667/0033-7587(2001)156[0577:CAFDTS]2.0.CO;2.

[22] Nikjoo H, Girard P. A model of the cell nucleus for DNA damage calculations. Int J Radiat Biol 2012;88:87–97. http://dx.doi.org/10.3109/09553002.2011.640860.

[23] Friedland W, Bernhardt P, Jacob P, Paretzke HG, Dingfelder M. Simulation of DNA damage after proton and low LET irradiation. Radiat Prot Dosim 2002;99:99–102.

[24] Kreipl MS, Friedland W, Paretzke HG. Interaction of ion tracks in spatial and temporal proximity. Radiat Environ Biophys 2009;48:349–59. http://dx.doi.org/10.1007/s00411-009-0234-z.

[25] Kreipl MS, Friedland W, Paretzke HG. Time- and space-resolved Monte Carlo study of water radiolysis for photon, electron and ion irradiation. Radiat Environ Biophys 2009;48:11–20. http://dx.doi.org/10.1007/s00411-008-0194-8.

[26] Meylan S. Development of a multi-scale simulation tool for early radio-induced damage assessment in cells exposed to light ions irradiations (proton and alpha). Université de Bordeaux; 2016.

[27] Lampe N. The long term impact of ionising radiation on living systems. Université Clermont Auvergne; 2017.

[28] Karamitros M, Mantero A, Incerti S, Friedland W, Baldacchino G, Barberet P, et al. Modeling radiation chemistry in the geant4 toolkit. Prog Nucl Sci Technol 2011;2:503–8.

[29] Karamitros M, Luan S, Bernal MA, Allison J, Baldacchino G, Davidkova M, et al. Diffusion-controlled reactions modeling in Geant4-DNA. J Comput Phys 2014;274:841–82. http://dx.doi.org/10.1016/j.jcp.2014.06.011. Elsevier Inc.

[30] Green NJB, Pilling MJ, Pimblott SM, Clifford P. Stochastic modeling of fast kinetics in a radiation track. J Phys Chem 1990;94:251–8. http://dx.doi.org/10.1021/j100364a041.

[31] Kyriakou I, Incerti S, Francis Z. Technical Note: Improvements in geant4 energy-loss model and the effect on low-energy electron transport in liquid water. Med Phys 2015;42:3870–6. http://dx.doi.org/10.1118/1.4921613. American Association of Physicists in Medicine.

[32] Bordage MC, Bordes J, Edel S, Terrissol M, Franceries X, Bardiès M, et al. Implementation of new physics models for low energy electrons in liquid water in Geant4-DNA. Phys Medica 2016;32:1833–40. http://dx.doi.org/10.1016/j.ejmp.2016.10.006.

[33] Tran HN, El Bitar Z, Champion C, Karamitros M, Bernal MA, Francis Z, et al. Modeling proton and alpha elastic scattering in liquid water in Geant4-DNA. Nucl Instr Methods Phys Res Sect B 2015;343:132–7. http://dx.doi.org/10.1016/j.nimb.2014.10.016. North-Holland.

[34] Kyriakou I, Sefl M, Nourry V, Incerti S. The impact of new Geant4-DNA cross section models on electron track structure simulations in liquid water. J Appl Phys 2016;119:194902. http://dx.doi.org/10.1063/1.4950808.

[35] Bordes J, Incerti S, Lampe N, Bardiès M, Bordage MC. Low-energy electron dose-point kernel simulations using new physics models implemented in Geant4-DNA. Nucl Instr Methods Phys Res Sect B 2017;398:13–20. http://dx.doi.org/10.1016/j.nimb.2017.02.044. North-Holland.

[36] Milligan JR, Aguilera JA, Ward JF. Variation of single-strand break yield with scavenger concentration for plasmid DNA irradiated in aqueous solution. Radiat Res 1993;133:151–7.

[37] Udovicić L, Mark F, Bothe E. Yields of single-strand breaks in double-stranded calf thymus DNA irradiated in aqueous solution in the presence of oxygen and scavengers. Radiat Res 1994;140:166–71. http://dx.doi.org/10.2307/3578899.

[38] Ward JF. DNA damage produced by ionizing radiation in mammalian cells: identities, mechanisms. Prog Nucleic Acid Res Mol Biol 1988;35:95–125.

[39] Pater P, Seuntjens J, El Naqa I, Bernal MA. On the consistency of Monte Carlo track structure DNA damage simulations. Med Phys 2014;41:121708. http://dx.doi.org/10.1118/1.4901555.

[40] Emfietzoglou D, Cucinotta FA, Nikjoo H. A complete dielectric response model for liquid water: a solution of the Bethe ridge problem. Radiat Res 2005;164:202–11.

[41] Watanabe N, Hayashi H, Udagawa Y. Inelastic X-ray scattering study on molecular liquids. J Phys Chem Solids 2000;61:407–9. http://dx.doi.org/10.1016/S0022-3697(99)00326-1. Pergamon.

[42] Hayashi H, Watanabe N, Udagawa Y, Kao C. The complete optical spectrum of liquid water measured by inelastic x-ray scattering. Proc Natl Acad Sci USA 2000;97:6264–6. http://dx.doi.org/10.1073/pnas.110572097. National Academy of Sciences.

[43] Emfietzoglou D, Nikjoo H. Accurate electron inelastic cross sections and stopping powers for liquid water over the 0.1-10 keV range based on an improved dielectric description of the Bethe surface. Radiat Res 2007;167:110–20. http://dx.doi.org/10.1667/RR0551.1.

[44] Liamsuwan T, Emfietzoglou D, Uehara S, Nikjoo H. Microdosimetry of low-energy electrons. Int J Radiat Biol 2012;88:899–907. http://dx.doi.org/10.3109/

09553002.2012.699136. Taylor & Francis.
[45] Emfietzoglou D, Papamichael G, Nikjoo H. Monte Carlo electron track structure calculations in liquid water using a new model dielectric response function. Radiat Res 2017;188:355–68. http://dx.doi.org/10.1667/RR14705.1. The Radiation Research Society.
[46] Barrios R, Skurski P, Simons J. Mechanism for damage to DNA by low-energy electrons. J Phys Chem B 2002;106:7991–4.
[47] Scholes G, Willson RL, Ebert M. Pulse radiolysis of aqueous solutions of deoxyribonucleotides and of DNA: reaction with hydroxy-radicals. J Chem Soc D Chem Commun 1969;17. http://dx.doi.org/10.1039/c29690000017. The Royal Society of Chemistry.
[48] Hirayama R, Ito A, Tomita M, Tsukada T, Yatagai F, Noguchi M, et al. Contributions of direct and indirect actions in cell killing by high-LET radiations. Radiat Res 2009;171:212–8.
[49] Daly MJ. Death by protein damage in irradiated cells. DNA Repair (Amst) 2012;11:12–21. http://dx.doi.org/10.1016/j.dnarep.2011.10.024. Elsevier B.V.
[50] de Lara CM, Hill MA, Jenner TJ, Papworth D, Neill PO. Dependence of the yield of DNA double-strand breaks in Chinese hamster V79–4 cells on the photon energy of ultrasoft X rays. Radiat Res 2001;155:440–8.
[51] Shiina T, Watanabe R, Shiraishi I, Suzuki M, Sugaya Y, Fujii K, et al. Induction of DNA damage, including abasic sites, in plasmid DNA by carbon ion and X-ray irradiation. Radiat Environ Biophys 2013;52:99–112. http://dx.doi.org/10.1007/s00411-012-0447-4.
[52] Nakano M, Tateishi-Karimata H, Tanaka S, Tama F, Miyashita O, Nakano S, et al. Local thermodynamics of the water molecules around single- and double-stranded DNA studied by grid inhomogeneous solvation theory. Chem Phys Lett 2016;660:250–5. http://dx.doi.org/10.1016/j.cplett.2016.08.032.
[53] Boudaiffa B, Cloutier P, Hunting D, Huels MA, Sanche L. Resonant Formation of DNA strand breaks by low-energy (3 to 20 eV) electrons. Science (80-) 2000;287:1658–61.
[54] Dingfelder M. Updated model for dielectric response function of liquid water. Appl Radiat Isot 2014;83:142–7. http://dx.doi.org/10.1016/j.apradiso.2013.01.016. Pergamon.
[55] Dingfelder M, Hantke D, Inokuti M, Paretzke HG. Electron inelastic-scattering cross sections in liquid water. Radiat Phys Chem 1999;53:1–18. http://dx.doi.org/10.1016/S0969-806X(97)00317-4. Pergamon.
[56] Kyriakou I, Sefl M, Nourry V, Incerti S. The impact of new Geant4-DNA cross section models on electron track structure simulations in liquid water. J Appl Phys 2016;119. http://dx.doi.org/10.1063/1.4950808.
[57] Emfietzoglou D, Nikjoo H. The effect of model approximations on single-collision distributions of low-energy electrons in liquid water. Radiat Res 2005;163:98–111. http://dx.doi.org/10.1667/RR3281.
[58] Roots R, Okada S. Estimation of life times and diffusion distances of radicals DNA strand breaks involved in X-ray-induced or killing of mammalian cells'. Radiat Res 1975;64:306–20.
[59] Balasubramanian B, Pogozelski WK, Tullius TD. DNA strand breaking by the hydroxyl radical is governed by the accessible surface areas of the hydrogen atoms of the DNA backbone. Proc Natl Acad Sci USA 1998;95:9738–43. http://dx.doi.org/10.1073/pnas.95.17.9738.
[60] Friedland W, Jacob P, Bernhardt P, Paretzke HG, Dingfelder M. Simulation of DNA damage after proton irradiation. Radiat Res 2003;159. http://dx.doi.org/10.1667/0033-7587(2003) 159[0401:SODDAP]2.0.CO;2. 410–410.
[61] Kellerer AM. Fundamentals of microdosimetry. In: Kase KR, Bjärngard BE, Attix FH, editors. The dosimetry of ionizing radiation. Academic Press; 1985. p. 77–162.
[62] Lampe N, Karamitros M, Breton V, Brown JMC, Sakata D, Sarramia D, et al. Mechanistic DNA damage simulations in geant4-DNA part 2: electron and proton damage in a realistic cellular geometry. Phys Medica 2017. http://dx.doi.org/10.1016/j.ejmp.2017.12.008.
[63] Lampe N, Biron DG, Brown JMC, Incerti S, Marin P, Maigne L, et al. Simulating the impact of the natural radiation background on bacterial systems: implications for very low radiation biological experiments. PLoS One 2016;11:1–19. http://dx.doi.org/10.1371/journal.pone.0166364.
[64] Santin G, Strul D, Lazaro D, Simon L, Krieguer M, Martins MV, et al. GATE: a geant4-based simulation platform for PET and SPECT integrating movement and time management. IEEE Trans Nucl Sci 2003;50:1516–21. http://dx.doi.org/10.1109/TNS.2003.817974.
[65] Buxton GV, Greenstock CL, Helman WP, Ross AB. Critical review of rate constants for reactions of hydrated electrons, hydrogen atoms and hydroxyl radicals (OH/O) in aqueous solution. J Phys Chem Ref Data 1988;17:513–886. http://dx.doi.org/10.1063/1.555805.